APPLICATION OF SEMI-LAGRANGIAN METHODS TO CLIMATE SIMULATION

D L Williamson
National Center for Atmospheric Research
Boulder, CO, USA

1. INTRODUCTION

All numerical approximations involve trade-offs among various advantages and disadvantages, and the semi-Lagrangian approach is no exception. Semi-Lagrangian methods have clear advantages for climate modeling, along with some disadvantages. However, the advantages outweigh the disadvantages. A supposed disadvantage with the semi-Lagrangian approach is a lack of a priori mass conservation. Various arbitrary fixers have been added to models to provide global mass conservation. They appear to be cosmetic, and to not interact with the physical parameterizations in any deleterious fashion (*Rasch and Williamson*, 1990, 1991, *Williamson and Rasch*, 1994, *Moorthi et al.*, 1995).

The advantages of the semi-Lagrangian approach include stability with long time steps, availability of two-time-level versions, suitability of linear grids, elimination of noise in the stratosphere, and a reduction of orographically locked precipitation. The last three will be illustrated in the following. We briefly mention the first two before presenting details of the others.

The potential for long time steps was the principal advantage which drove the development of semi-Lagrangian methods for high resolution numerical weather prediction (see the review by *Staniforth and Côté*, 1991). The time step is less of an advantage for climate models at the resolutions commonly employed today, but will become more important in the future as modeling groups move to higher resolution. Currently, spectral semi-implicit Eulerian climate models applied at T42 or lower truncations, use a time step of 20 minutes or longer ($2\Delta t$ of 40 minutes). Many physical parameterizations in these models are not designed for application over periods longer than 1 hour (and in some instances require modification for application at 1 hour). Thus, the time step of coarse resolution climate models cannot be appreciably lengthened. In addition, the saving due to the modest increase implied above is partially offset by increased computation required by the semi-Lagrangian approximations. For example, the T42 semi-Lagrangian version of the NCAR Community Climate Model, CCM2 (*Williamson and Olson*, 1994) with a 30 minute time step requires the same computing resources as the T42 Eulerian version with its standard 20 minute time step, both applied on a quadratically unaliased (128 x 64 point) grid. The long time step advantage will only be realizable at higher resolutions with the time step held at 30 minutes. We will show below that the vertical resolution must also be above some minimum for semi-Lagrangian schemes to be advantageous.

Two-time-level schemes offer a potential savings of 50% over three-time-level schemes (again see the review by *Staniforth and Côté*, 1991; *Bates et al.*, 1993; and more specifically for application to spectral transform models, see *Temperton*, elsewhere in this workshop report). However, the actual savings are likely to be less. For example, since the radiation calculation is not done every time step in the CCM2, but rather at 1 hour intervals (*Hack et al.*, 1993), and consumes 50% of the computer time, the actual savings with CCM2 will more realistically be 25%. Two-time-level schemes, however, are also attractive because they are more consistent with tracer transport in climate models where a centered time level plays no role in constituent interaction calculations.

In the following we first review the advantages of linear grids with semi-Lagrangian approximations. We then show the basic difference in the simulated climates with Eulerian and semi-Lagrangian dynamics in a preliminary version of CCM3. To help interpret this difference we examine the convergence with increasing vertical resolution of semi-Lagrangian and Eulerian approximations using the simplified, idealized forcing of *Held and Suarez* (1994). Finally, we consider spurious mountain resonance and demonstrate that the *Ritchie and Tanguay* (1996) modification to eliminate this resonance also reduces the spurious orographic precipitation common to atmospheric general circulation models.

2. LINEAR GRID

Eulerian, global, baroclinic spectral transform models generally adopt quadratic unaliased computational Gaussian grids. The *quadratic* grid is defined to be the minimum grid for which the transform of the product of two fields, each of which is representable in spectral space, has no aliasing onto the waves of the underlying spectral representation. Such grids are chosen to prevent nonlinear instability associated with Eulerian advection approximations. Grids coarser than quadratic tend to lead to instability in Eulerian baroclinic models. *Côté and Staniforth* (1988) suggested that a linear grid might be suitable for semi-Lagrangian spectral transform models. The *linear grid* is defined to be the minimum grid required for transformations of a field from spectral space to grid point space and back to spectral again without loss of information. With such a grid, only linear terms are unaliased. *Côté and Staniforth* (1988) explored the use of a linear grid experimentally in the shallow water equation framework. They showed that in the shallow water context a linear grid gave 5-day forecasts of comparable quality to forecasts with a quadratic grid.

Williamson (1996) considered the suitability of linear grids for atmospheric general circulation modeling by examining a series of climate simulations with the semi-Lagrangian version of the NCAR CCM2 (*Williamson and Olson*, 1994) at different horizontal spectral resolutions with linear and quadratic grids. He showed that linear grids present no problems for climate simulations with semi-Lagrangian, spectral transform models. The spectral truncation, rather than the transform grid on which the physical parameterizations are calculated,

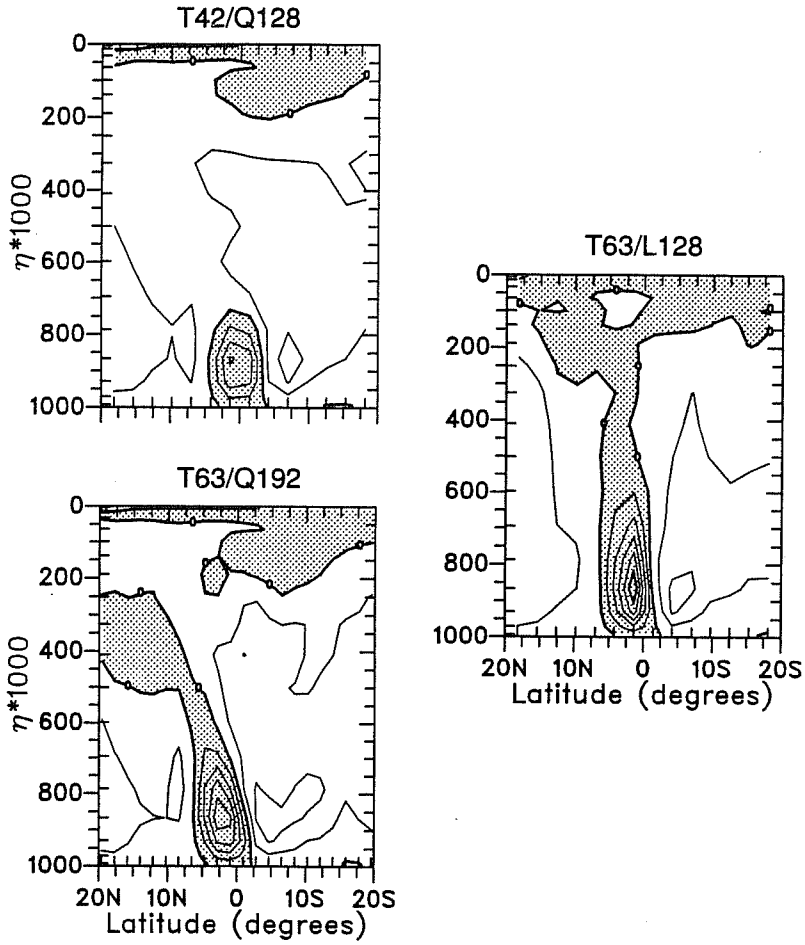

Fig. 1 January average, zonal average over Atlantic (30° W to 75° E) pressure vertical velocity (ω) for T42/Q128, T63/Q192, and T63/L128 simulations. Contour interval is 20 mb day^{-1}, negative (upward) regions stippled. Averages are taken on model (η) surfaces and η*1000 corresponds approximately to pressure in mb.

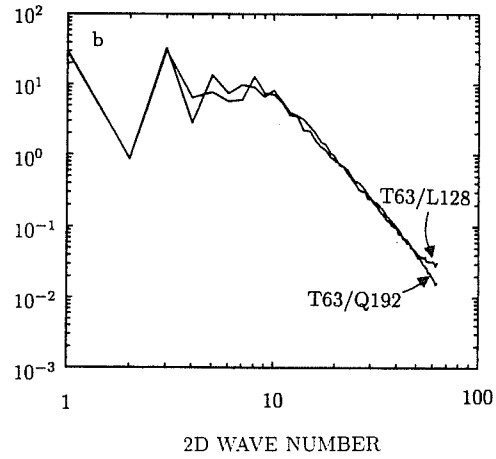

Fig. 2 January average kinetic energy spectra (total kinetic energy versus spherical wave number) at 500 mb from T63/Q192 and T63/L128 simulations.

dominates the accuracy of simulations. This conclusion is illustrated in Fig. 1 which shows the pressure vertical velocity, ω, in the tropics, zonally averaged over the Atlantic ocean (30W longitude to 5E longitude). The simulations are referenced by the spectral truncation and number of longitudinal grid points, including L and Q as a reminder for which type of grid is employed. Thus the simulations on quadratic grids are referred to as T42/Q128 and T63/Q192. That on the linear grid is referred to as T63/L128. Fig. 1 can be compared with Fig. 6 in *Williamson et al.*, (1995) which shows the same fields from a series of simulations with the Eulerian CCM2 at resolutions R15 through T106. The semi-Lagrangian simulations with the quadratic grids (left column, Fig. 1) show the same resolution signal as the Eulerian. The strength, width, and depth of the upward cell ($\omega < 0$) all vary with resolution. The accompanying subsidence regions also show dependence on resolution. The T42/Q128 simulation shows a weak, shallow cell of upward motion. The T63/Q192 simulation shows a significant increase in vertical extent and strength of the upward cell with central values are almost double those in the T42/Q128. The T63/L128 simulation has the characteristics of the T63/Q192 rather than the T42/Q128. The upward branch is stronger and extends throughout the troposphere.

The zonal averages illustrate the advantages of the linear grid. However, small scale, spatial noise might accumulate with the linear grids to create a problem. This is not the case as illustrated in Fig. 2 which shows the 500mb kinetic energy spectra as a function of two-dimensional wavenumber for the T63/L128 and T63/Q192 simulations, both averaged for January. The two simulations use the same horizontal diffusion coefficient. The T63/L128 shows an increase in energy for wavenumbers above 50 compared to the T63/Q192. This difference is comparable to that found between the Eulerian and semi-Lagrangian versions, and to that which occurs when the diffusion coefficient is halved or doubled (both examples are shown in Fig. 2 of *Williamson and Olson*, 1994). The increase in kinetic energy above wavenumber 50 in the T63/L128 simulation occurs gradually throughout the first four months of the simulation, after which the monthly average spectrum above wavenumber 10 does not change. The differences below wavenumber 10 seen in Fig. 2, are comparable to the year-to-year differences that occur in the Eulerian CCM2 in long control integrations. Additional details of the simulations with linear grids are provided in *Williamson* (1996).

An additional potential advantage of linear grids, not discussed here, is that the grid and spectral space are more commensurate, and problems associated with spectral ringing may be minimized.

3. VERTICAL RESOLUTION

Fig. 3a shows the basic signal in the zonal mean temperatures associated with the change from Eulerian to semi-Lagrangian dynamical approximations. The figure shows the difference (semi-Lagrangian minus Eulerian) between simulations based on a preliminary version of CCM3 in which the physical parameterizations have been improved over those in CCM2, with T42 spectral truncation and 18 levels. The

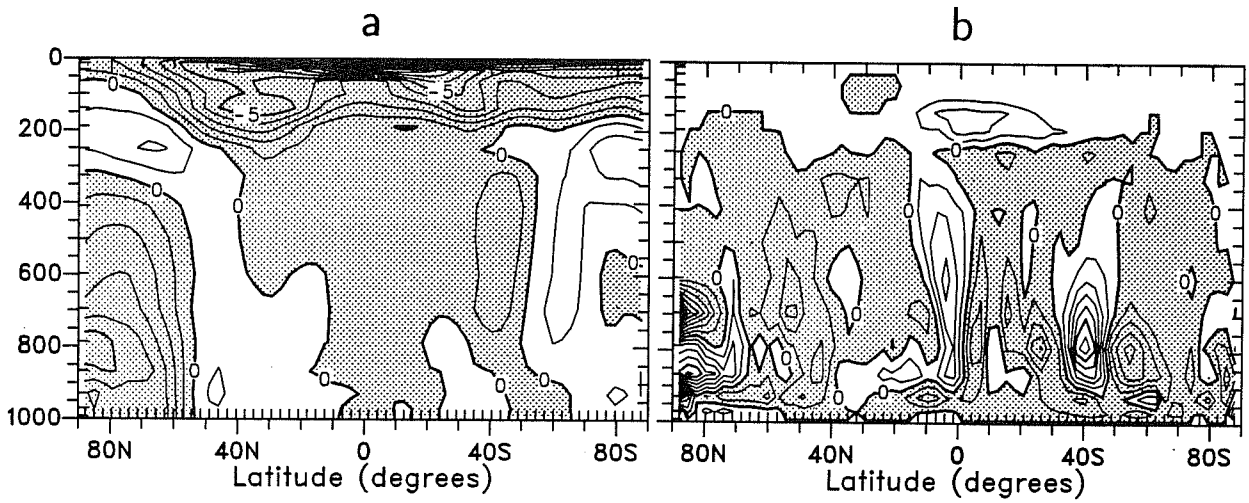

Fig. 3 January average, zonal average difference (semi-Lagrangian minus Eulerian) of (a) temperature and (b) convective mass flux. Contour intervals are 1.0 K and 5.0 mb/day, respectively.

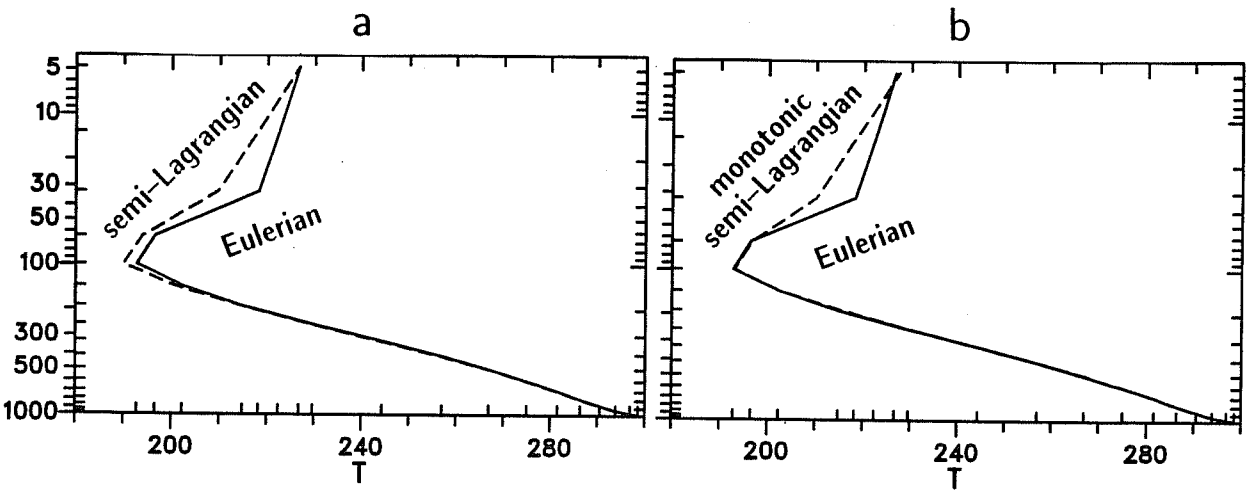

Fig. 4 January average, zonal average temperature profiles averaged from 7 S to 7 N from (a) Eulerian (solid) and semi-Lagrangian (dashed) and (b) Eulerian (solid) and monotonic semi-Lagrangian (dashed).

difference essentially shows the same signal that was seen with the frozen CCM2 simulations (*Williamson and Olson*, 1994). The new parameterizations, while changing the individual simulated climates, have little effect on the difference. The polar tropopause is warmer with semi-Lagrangian approximations, and the tropical tropopause, stratosphere and north polar troposphere are colder. The warmer polar tropopause is desirable, ameliorating a common bias in models (*Boer et al.*, 1992), and has been observed with other semi-Lagrangian climate models (*Chen and Bates*, 1996). The colder North polar troposphere, which is undesirable, is caused by a reduction of high clouds associated with decreased relative humidity in the tropopause region, which results from the increased tropopause temperature (the specific humidity shows little change in that region, but if anything, decreases somewhat). It is reasonable to eliminate the change in north polar tropospheric temperature by adjusting the diagnostic cloud parameterization to compensate for the decreased relative humidity in the vicinity of the tropopause. The parameters in the diagnostic cloud scheme were originally chosen in the Eulerian version so that the simulation provided a good match to ERBE data.

The decreased tropical tropopause temperature is also undesirable since the Eulerian version produced a tropical tropopause temperature and location close to observed. Accompanying the colder tropopause is an increase in the convective mass flux seen in Fig. 3b. In the difference the increase appears to be a shallow cycling below the tropopause, only weakly connected to the increased deep upward flux. By means of some complex interaction, the temperature decreases, the convective mass flux increases, the specific humidity decreases but relatively less than the temperature so both the relative humidity and clouds increase. The increased clouds emit less long wave radiation (than the surface) for the stratospheric ozone to absorb, leading to the colder stratosphere as well.

The tropical mean temperature profiles are shown in Fig. 4a for the Eulerian and semi-Lagrangian simulations. Fig. 4b shows the profile for a simulation with the semi-Lagrangian method using monotonic interpolants. Although the tropopause temperature in the monotonic semi-Lagrangian simulation matches that of the Eulerian, the stratosphere remains colder indicating that the model processes may be behaving like the non-monotonic semi-Lagrangian version of Fig. 4a. That is in fact the case. Although the tropopause temperature in the monotonic semi-Lagrangian simulation is the same as that in the Eulerian, the convective mass flux has increased below the tropopause and the clouds have increased, just as in the non-monotonic case.

It is very difficult to diagnose cause and effect associated with the numerical approximations in the complex system provided by the complete model, especially as the primary balance in the tropical troposphere is convective-radiative, with the dynamics and hence numerical approximation playing a secondary role.

Therefore, to isolate the numerical aspects, we examine the differences between semi-Lagrangian and Eulerian approaches in the simpler, idealized dynamical core framework of *Held and Suarez* (1994).

Figs. 5a and b show the tropical temperature profiles from T42 semi-Lagrangian and Eulerian simulations, respectively, with 18, 36 and 72 vertical levels. Both methods converge with increasing vertical resolution with a tropopause forming around 140 mb. The Eulerian appears to have converged with 18 levels while the semi-Lagrangian has not. The 18-level, semi-Lagrangian simulation forms the tropopause 1 level higher (99 mb) and about 7 K colder than the 36 and 72 level simulations. The 18-level Eulerian simulation, however, doesn't quite capture the single level tropopause structure implied by the 36 and 72 level Eulerian simulations. The minimum value occurs at both 140 mb and 99 mb, but both values are close to the 188K of the higher resolution simulations. This is seen more clearly in the following figure.

Figs. 6a-c show that the Eulerian and semi-Lagrangian simulations converge to the same tropopause structure with 72 levels, although the structures in the stratosphere near the top of the model differ. The difference there is presumably due to different advection top boundary conditions in the Eulerian and semi-Lagrangian schemes. Figs. 6b and c show a hint of vertical grid scale noise in the stratosphere in the Eulerian simulation. This noise is seen more clearly in Fig. 7b for both T42 and T63 simulations. The noise is not seen in the corresponding semi-Lagrangian simulations (Fig. 7a). Fig. 7 also shows that the T63 simulations have slightly colder tropopause temperatures than the T42 simulations. This is also the case with 18 and 72 levels (not shown). In addition, the T95 semi-Lagrangian simulation produces a colder tropical tropopause than the T63 semi-Lagrangian (also not shown).

Fig. 8 compares the 18-level, semi-Lagrangian simulation (shown previously in Fig. 5a) which used a Lagrange cubic polynomial interpolant, with one using a monotonic Hermite cubic polynomial interpolant. The monotonic interpolant produces a warmer troposphere, but it is still colder than the Eulerian or the higher vertical resolution simulations. This explains the puzzling results seen earlier in Fig. 4b with the full model in which the tropopause temperature matched that of the Eulerian simulation, but the monotonic semi-Lagrangian still had extra convective activity there and associated increased clouds. Both 18-level monotonic and non-monotonic semi-Lagrangian versions produce a colder tropopause than the Eulerian, stimulating extra convection and associated heating at the tropopause level. In the monotonic version this extra heating is fortuitously sufficient to bring the temperature to the Eulerian value, while in the non-monotonic version it stays below.

The simulations with the idealized Held-Suarez forcing imply that extra resolution above that in the 18-level CCM2 is needed in the vicinity of the tropopause with the three-dimensional semi-Lagrangian approximations.

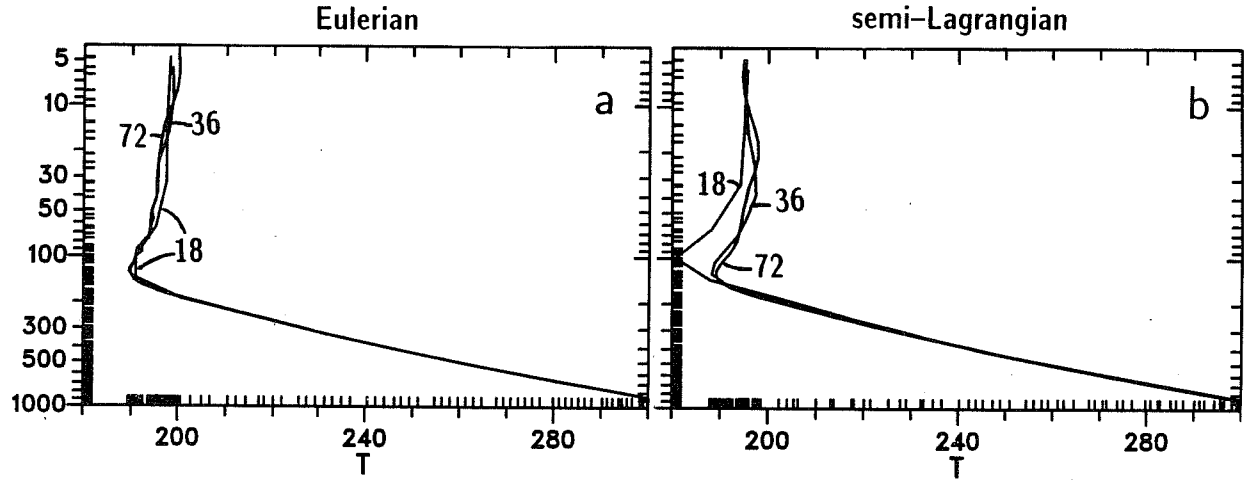

Fig. 5 Zonal average temperature profiles averaged from 7 S to 7 N from Held-Suarez test case with 18, 36, and 72 levels. (a) T42 Eulerian and (b) T42 semi-Lagrangian.

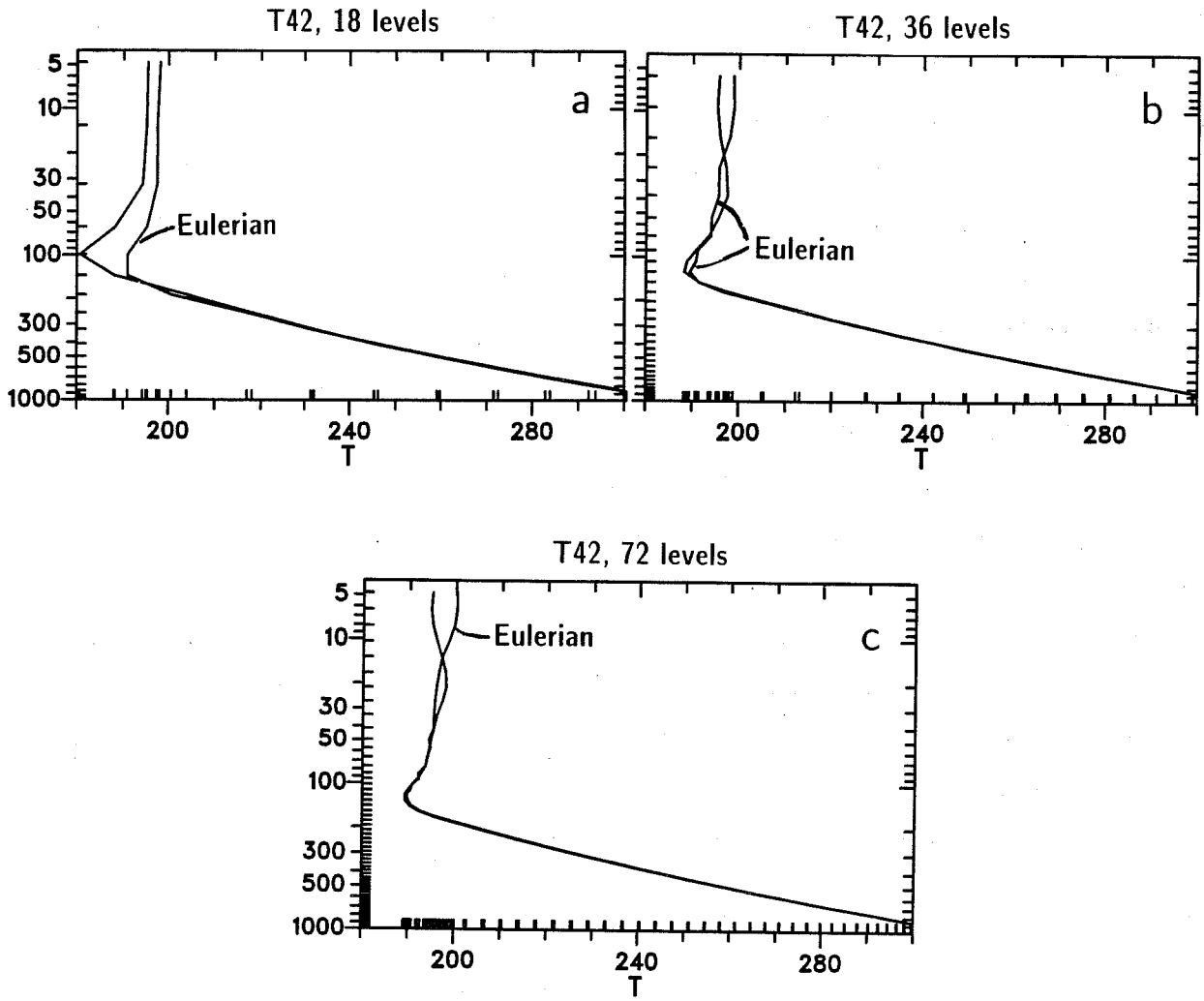

Fig. 6 Zonal average temperature profiles averaged from 7 S to 7 N from Held-Suarez test case for T42 Eulerian and semi-Lagrangian simulations. (a) 18 levels, (b) 36 levels, and (c) 72 levels.

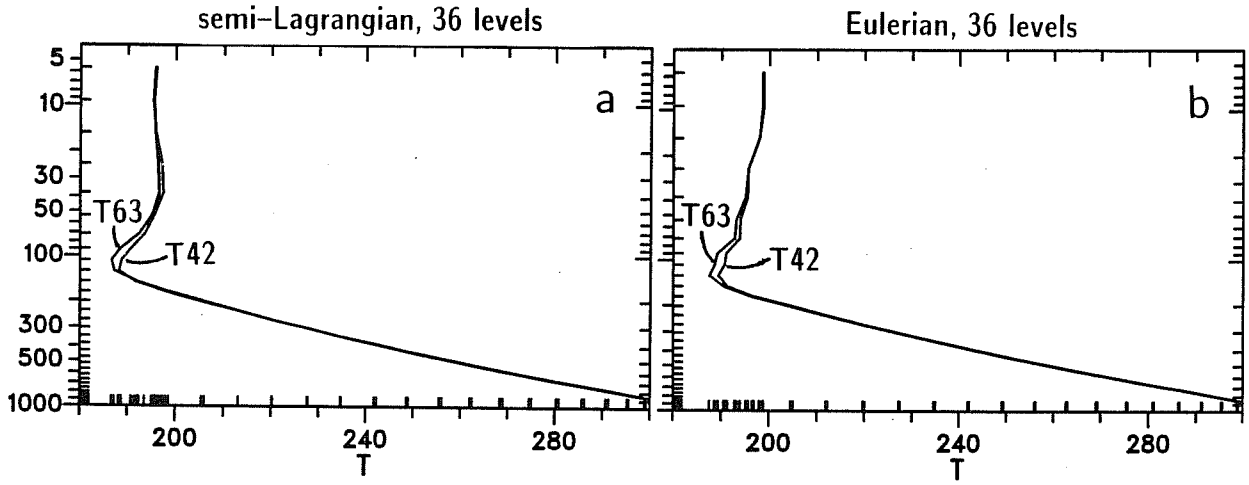

Fig. 7 Zonal average temperature profiles averaged from 7 S to 7 N from Held-Suarez test case for 36 level T42 and T63 simulations. (a) semi-Lagrangian, and (b) Eulerian.

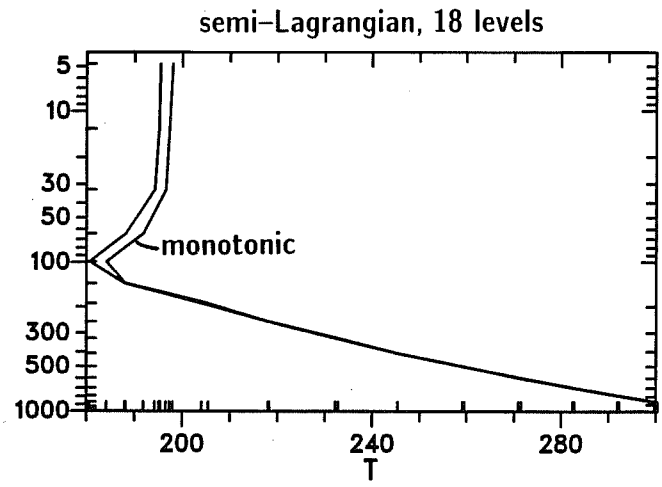

Fig. 8 Zonal average temperature profiles averaged from 7 S to 7 N from Held-Suarez test case for 18 level T42 semi-Lagrangian simulations with cubic polynomial and monotonic interpolants.

Therefore, as a stopgap until we increase the vertical resolution, we adopt the non-interpolating-in-the-vertical strategy of *Ritchie* (1991). This version produces a tropical tropopause matching that of the Eulerian without the increased mass flux of the three-dimensional semi-Lagrangian version, but continues to produce the desirable warmer polar tropopause. We have modified the diagnostic cloud parameterization slightly to compensate and reduce the polar troposphere cold bias seen in Fig. 3a. Fig. 9 compares the zonal average temperatures of the semi-Lagrangian and Eulerian versions. The figure shows the model temperature biases against the ECMWF analyses (model minus analysis) for Dec-Jan-Feb (top row) and Jun-Jul-Aug (bottom row). The Eulerian model is T42 on the quadratic (164 x 32 point) grid and the semi-Lagrangian is T63 on the linear (164 x 32 point) grid. The general characteristics of these difference fields are very similar; however, the semi-Lagrangian has slightly smaller tropical troposphere cold bias and smaller polar tropopause cold biases in both seasons.

4. OROGRAPHIC ASPECTS

The T63, linear grid, Δt = 30 min, non-interpolating-in-the-vertical semi-Lagrangian model is subject to spurious orographic resonance (*Rivest et al.*, 1994), although it is not obvious in the climate statistics. The resonant states tend to be rare events lasting only a few days and thus are masked in monthly average statistics. Nevertheless the resonance must be eliminated. We have implemented the 1st order off-centering of *Rivest et al.* (1994), the 2nd order, four-time-level off-centering of *Rivest and Staniforth* (1995) and the Eulerian treatment of mountains *of Ritchie and Tanguay* (1996 and elsewhere in this meeting report). All methods result in essentially the same zonal averaged means; however, there are some disadvantages and advantages associated with certain of these approaches.

Fig. 10 shows the global averaged eddy kinetic energy for the T42, Δt = 20, quadratic grid simulation, and various T63, Δt = 30, linear grid simulations. The 1st order off-centering of *Rivest et al.* (1994) with a coefficient of 0.4 produces a significant reduction of the eddy kinetic energy. The 2nd order off-centering of *Rivest and Staniforth* (1995) with a coefficient of 1/3 (not shown) produces a similar reduction in eddy kinetic energy. Such large off-centering coefficients, which guarantee the elimination of the spurious resonance for all time steps, are not needed with the T63, Δt = 30 simulations however. A value of 0.1 for the *Rivest et al.* (1994) off-centering eliminates the spurious resonance without reducing the eddy kinetic energy. In fact, the eddy kinetic energy is increased somewhat in the middle and upper troposphere. With the approach of *Ritchie and Tanguay* (1996) and an off-centering coefficient of 0.1, which also guarantees the elimination of the spurious resonance for all time steps, the eddy kinetic energy is damped somewhat around the level of the jet maximum, but not as much as with the *Rivest et al.* (1994) off-centering with a coefficient of 0.4. However the approach of *Ritchie and Tanguay* (1996) has other advantages to be discussed next.

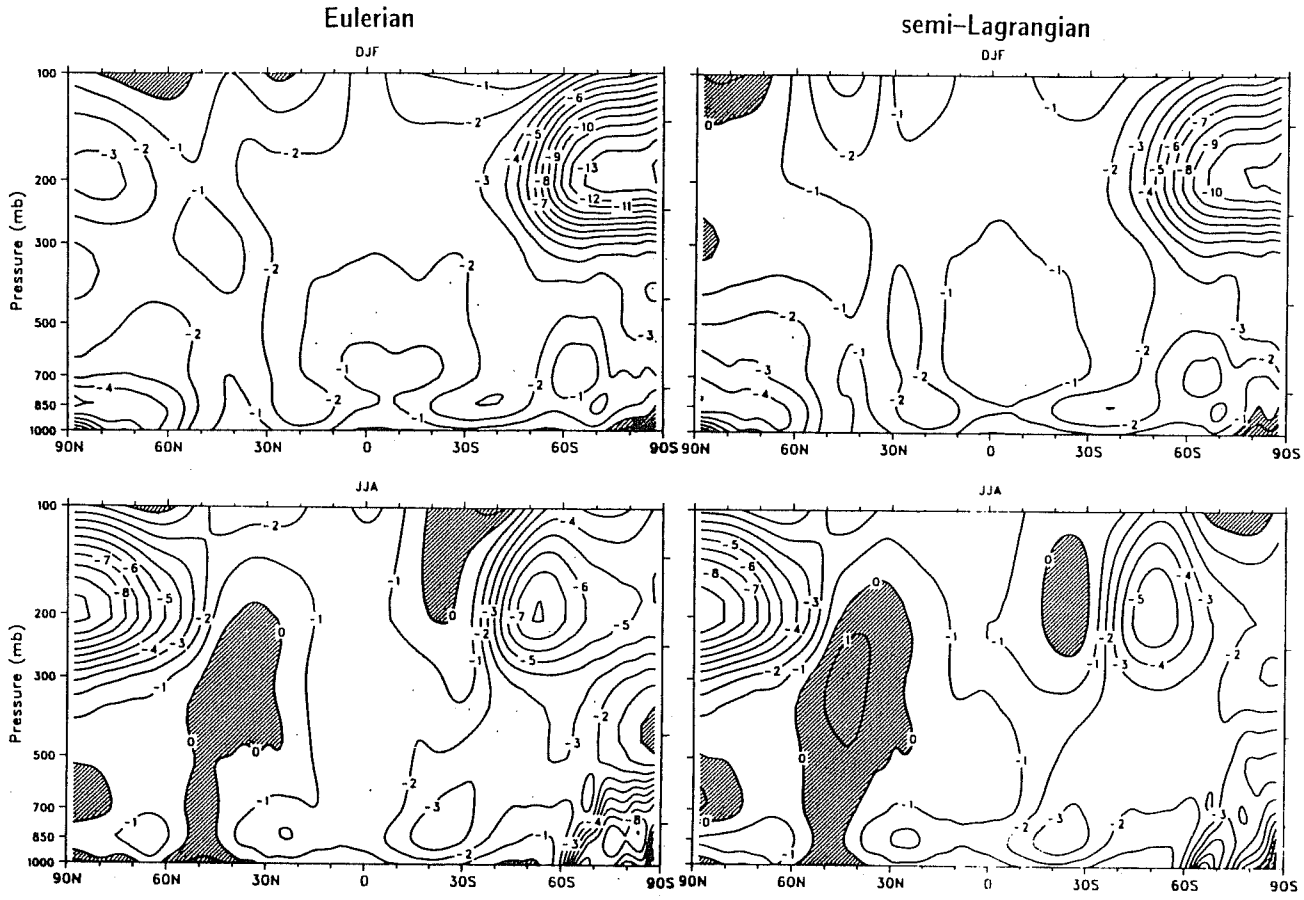

Fig. 9 January average, zonal average temperature differences (model minus ECMWF analyses). Top row for Dec-Jan-Feb, bottom row for Jun-Jul-Aug. Left column for Eulerian, right column for semi-Lagrangian. Contour interval is 1.0 K, positive differences shaded.

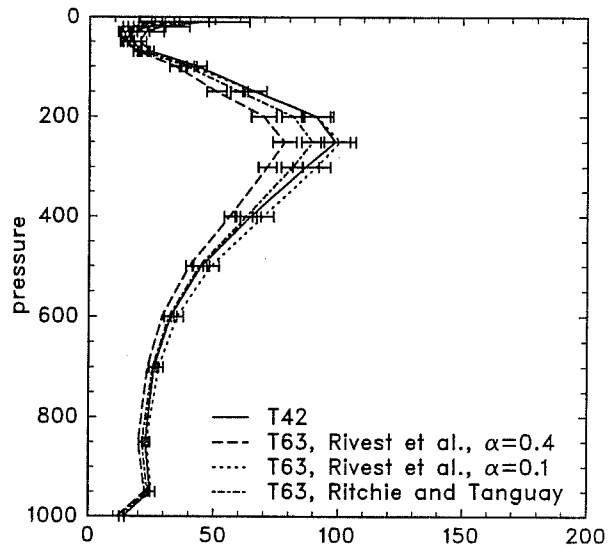

Fig. 10 January averaged, global average eddy kinetic energy from semi-Lagrangian simulations. Horizontal bars denote the standard deviation of monthly averages. See text for details of the cases.

Orographically locked precipitation is a common problem in models. It is illustrated in Fig. 11 which shows the January average precipitation over South America from T42 Eulerian and semi-Lagrangian variants (a and b, respectively) of a preliminary version of CCM3. A spurious precipitation maximum occurs on the eastern flank of the Andes, and the flow field is distorted to flux the water vapor away from the true convergence region to the spurious one on the mountain flank. The T63, linear grid semi-Lagrangian simulation (Fig. 11c) shows a similar, if not more exaggerated problem. In this simulation, the orography is truncated at T63 and has higher peaks and steeper slopes. The precipitation also shows smaller scale structures because the temperature and convergence are not spectrally filtered as strongly with the linear grid. (Water vapor is treated identically in the T42 quadratic and T63 linear versions since it is not spectrally truncated.) Fig. 11d shows the precipitation for the T63, linear grid semi-Lagrangian simulation when the model is modified to include the *Ritchie and Tanguay* (1996) Eulerian treatment of mountains. The spurious mountain precipitation is significantly reduced. The moisture flux is no longer distorted and the precipitation maximum occurs much closer to where it is observed over Brazil, although it exceeds climatological estimates.

Fig. 12 shows the July averaged precipitation over India and the Tibetan plateau. Again, the T42 Eulerian and semi-Lagrangian simulations (a and b, respectively) show the precipitation forming spuriously on the southern flank of the Himalayan mountains. The problem is exacerbated with the higher resolution orography of the T63 linear grid (Fig. 12c). Once again, the water vapor flux is distorted and the moisture is drawn away from the region where the precipitation is observed to occur. Fig. 12d shows the precipitation from the T63 version with the *Ritchie and Tanguay* (1996) approach. The precipitation on the flank of the mountains is reduced significantly. Again the distortion of the water vapor flux by the orography is reduced allowing the precipitation to form elsewhere.

5. CONCLUSIONS

The semi-Lagrangian method is very good for climate modeling. It offers economical advantages and reduces several persistent errors in the simulated climates. The savings from long time steps can be achieved at resolutions above T42 when the Eulerian time step restriction would be well below the 1 hour bound commonly imposed by the physical parameterizations. The semi-Lagrangian approximations are stable with a linear grid and thus provide a 50% increase in longitudinal and latitudinal resolution over Eulerian models at negligible additional cost. The linear grid also lessons the spectral ringing problem which occurs in spectral transform models. The two-time-level approach described by *Temperton* (elsewhere in this report) will provide another reduction in computer time of around 25% in climate model applications, where radiation is done less frequently then every time step, but still consumes around 50% of the total resources. The two-time-level approach is also more consistent with applications involving transported constituents (e.g. chemistry)

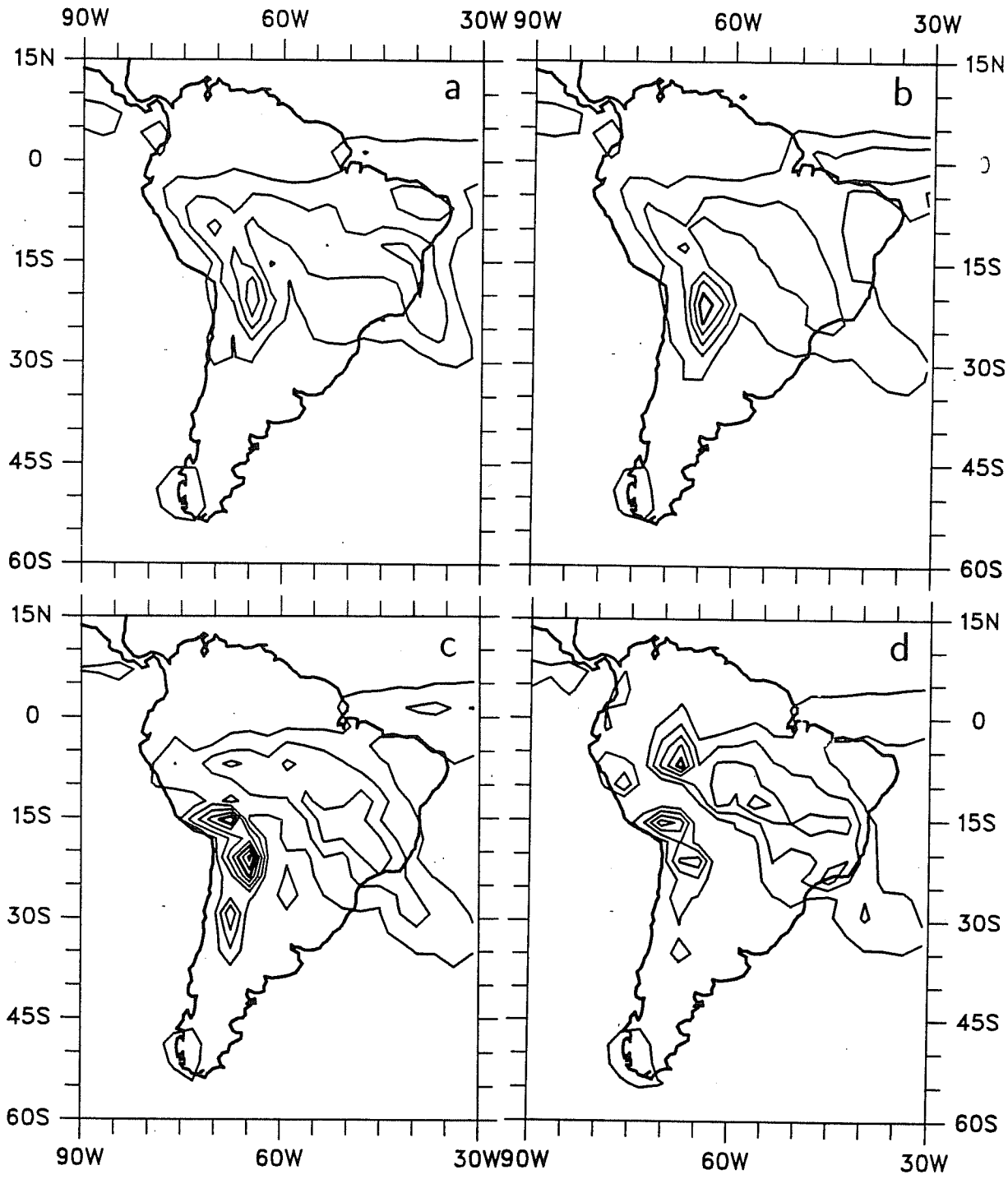

Fig. 11 January average precipitation over South America from (a) Eulerian, T42 quadratic grid, (b) semi-Lagrangian, T42 quadratic grid, (c) semi-Lagrangian, T63 linear grid, and (d) semi-Lagrangian, T63 linear grid with Ritchie and Tanguay approach. Contour interval is 5 mm/day.

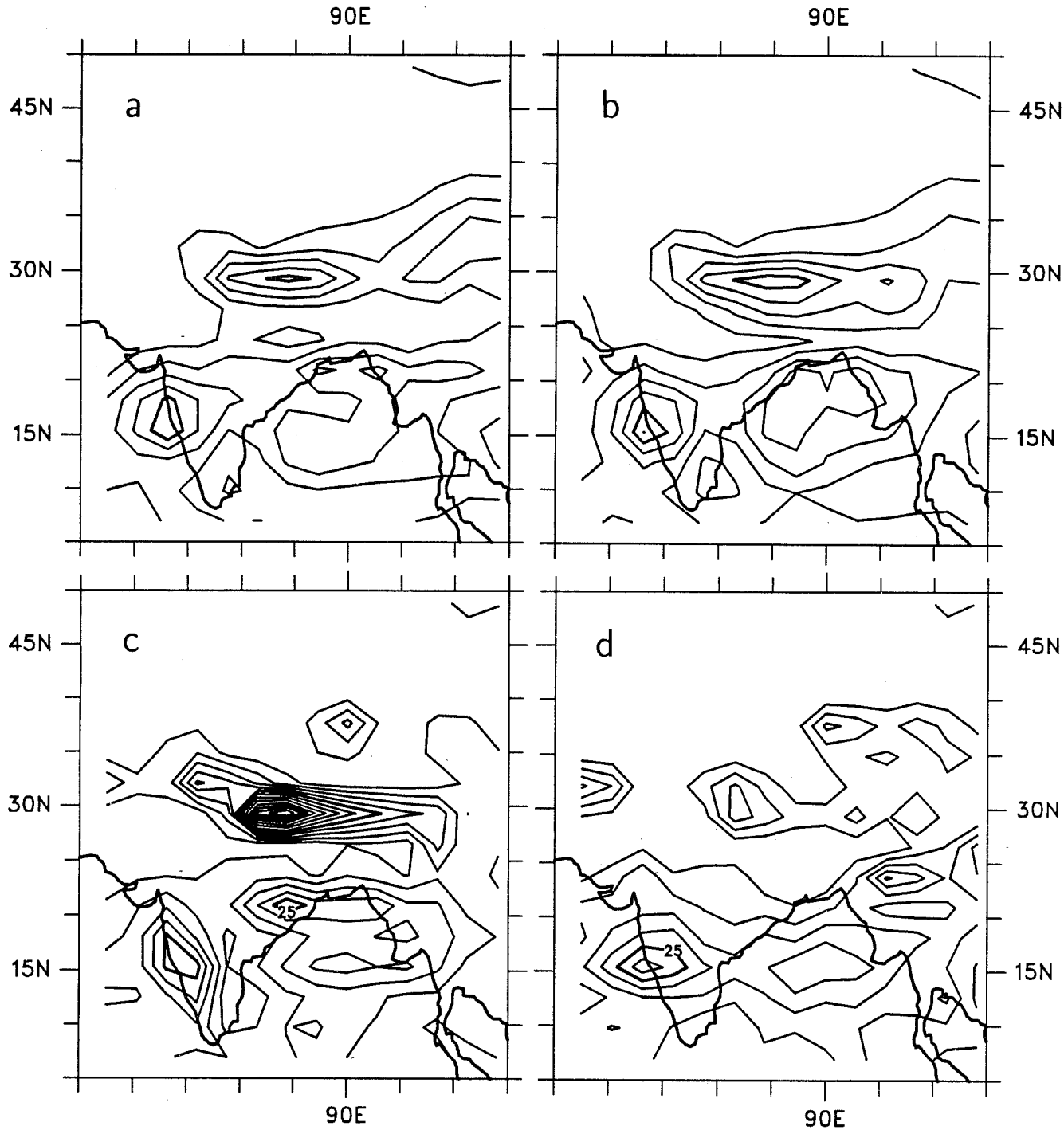

Fig. 12 July average precipitation over Indian sub-continent from (a) Eulerian, T42 quadratic grid, (b) semi-Lagrangian, T42 quadratic grid, (c) semi-Lagrangian, T63 linear grid, and (d) semi-Lagrangian, T63 linear grid with Ritchie and Tanguay approach. Contour interval is 5 mm/day.

where the center time level does not enter the equations, and the three-time-level approach predicts two uncoupled, interlaced time sequences requiring application of a time filter.

The semi-Lagrangian approximations produce a warmer polar tropopause than the Eulerian, reducing a common model bias. This improvement, however, tends to reduce the relative humidity there and thus the high clouds in the polar regions, which in turn produce lower tropospheric polar temperatures. The diagnostic cloud parameterization must be adjusted to compensate for this. The semi-Lagrangian approximations do not exhibit the stationary, vertical grid scale noise seen in the stratosphere with Eulerian schemes at higher vertical resolution. Finally, orographically locked precipitation is substantially reduced with semi-Lagrangian schemes employing the *Ritchie and Tanguay* (1996) Eulerian treatment of mountains. The distortion of the water vapor flux is substantially reduced allowing precipitation to occur closer to where it is observed to occur.

ACKNOWLEDGMENTS

I would like to thank Jerry Olson for developing the semi-Lagrangian codes and running the experiments described in this paper, Jim Hurrell for making Fig. 9, and Paula Drager for editorial improvements. This work was partially supported by the Computer Hardware, Advanced Mathematics, and Model Physics (CHAMMP) Program which is administered by the Office of Energy Research under the Office of Health and Environmental Research in the US Department of Energy, Environmental Sciences Division. The National Center for Atmospheric Research is sponsored by the National Science Foundation.

REFERENCES

Bates, J R, S Moorthi, and R W Higgins, 1993: A global multilevel atmospheric model using a vector semi-Lagrangian finite difference scheme. Part I: Adiabatic formulation. Mon Wea Rev 121, 244-263.

Boer, G J, K Arpe, M Blackburn, M Deque, W L Gates, T L Hart, H L Treut, E Roeckner, D A Sheinin, I Simmonds, R N B Smith, T Tokioka, R T Weatherald, and D Williamson, 1992: Some results from an intercomparison of the climates simulated by 14 atmospheric general circulation models. J Geophys Res 97, 12771-12786.

Chen, M and J R Bates, 1996: An intercomparison of climate simulations from a semi-Lagrangian and an Eulerian GCM. J Climate, submitted.

Côté, J and A Staniforth, 1988: A Two-time-level semi-Lagrangian semi-implicit scheme for spectral models. Mon Wea Rev 116, 2003-2012.

Hack, J J, B A Boville, B P Briegleb, J T Kiehl, P J Rasch, and D L Williamson, 1993: Description of the NCAR Community Climate Model (CCM2). *NCAR Technical Note* NCAR/TN-382+STR, 108pp.

Held, I M and M J Suarez, 1994: A proposal for the intercomparison of the dynamical cores of atmospheric general circulation models. Bull Amer Meteor Soc 75, 1825-1830.

Moorthi, S, R W Higgins, and J R Bates, 1995: A global multilevel model using a vector semi-Lagrangian finite-difference scheme. Part II: Version with physics. Mon Wea Rev 123, 1523-1541.

Rasch, P J, and D L Williamson, 1990: Computational aspects of moisture transport in global models of the atmosphere. Quart J Roy Meteor Soc 116, 1071-1090.

Rasch, P J, and D L Williamson, 1991: The sensitivity of a general circulation model climate to the moisture transport formulation. J Geophys Res 96, 13,123-13,137.

Ritchie, H, 1991: Application of the semi-Lagrangian method to a multilevel spectral primitive-equations model. Quart J Roy Meteor Soc 117, 91-106.

Ritchie, H and M Tanguay, 1996: A comparison of spatially-averaged Eulerian and semi-Lagrangian treatments of mountains. Mon Wea Rev, submitted.

Rivest, C and A Staniforth, 1995: Modifying the conventional three-time-level semi-implicit semi-Lagrangian scheme to eliminate orographically-induced spurious resonance. Atmosphere-Ocean 33, 109-119.

Rivest, C, A Staniforth, and A Robert, 1994: Spurious resonant response of semi-Lagrangian discretizations to orographic forcing: diagnosis and solution. Mon Wea Rev 122, 366-376.

Staniforth, A and J Côté, 1991: Semi-Lagrangian integration schemes for atmospheric models - A Review. Mon Wea Rev 119, 2206-2223.

Williamson, D L, and P J Rasch, 1994: Water vapor transport in the NCAR CCM2. Tellus 46A, 34-51.

Williamson, D L, 1996: Climate simulations with a spectral, semi-Lagrangian model with linear grids. Atmosphere-Ocean, in press.

Williamson, D L, J T Kiehl, and J J Hack, 1995: Climate sensitivity of the NCAR Community Climate Model (CCM2) to horizontal resolution. Clim Dynamics 11, 377-397.